Chapter 3

PASSIVE METHOD FOR ISLANDING DETECTION USING VARIATIONAL MODE DECOMPOSITION

3.1 INTRODUCTION

As the distributed energy resources penetration level increases, the distribution system operator faces the challenging task of unintentional islanding detection. Besides, islanding detection schemes are affected due to the presence of different types of distributed generation systems and intelligent inverters. The presence of these devices hinders the capability of islanding detection schemes [3]. This study proposes a practical methodology of variational mode decomposition-based energy index for islanding detection to mitigate these issues. It is an entirely intrinsic, adaptive, and variational method.

This chapter proposes a VMD-based IDT for ascertaining the islanding and non-islanding conditions due to its distinct properties. VMD is an entirely intrinsic approach, and it has an excellent signal analyzing capability. It can decompose the multicomponent signal into a finite number of band-limited intrinsic mode functions (IMFs) [93]. This study introduces a VMD-based islanding detection methodology for multiple and mixed-type grid-connected distributed generators. The research includes the impact of both inverter-type and synchronous-type DG systems, which has not been very commonly addressed. The main contribution of the chapter can be summarised as follows:

- This chapter proposes a noise-resistant IDT mechanism. The efficacy of the proposed VMD-based IDT is not affected by the presence of external noise.

- The proposed method is capable of reducing the NDZ and discriminating islanding in the case of zero power mismatch conditions.
- In the case of the zero power mismatch condition, the proposed method discriminates islanding within 0.12 s (six cycles). The proposed IDT can distinguish islanding and non-islanding conditions under highly vulnerable conditions such as three-phase ground (LLLG) fault, capacitor switching, and induction machine switching transients with enough margin.

The present chapter has been organized into five sections. The basic principles of functioning of the proposed VMD method for islanding detection have been described in Section 3.2. The implementation of the proposed method through simulation has been presented in Section 3.3. The actual simulation results are discussed in Section 3.4, which authenticates the islanding detection capability of the proposed method. Finally, the present investigation findings are enumerated in the conclusion in Section 3.5.

3.2 VMD: OVERVIEW

VMD has emerged as a robust, noise immune, and non-recursive scheme for signal processing. It acts as an entirely intrinsic, adaptive, and quasi-orthogonal decomposition tool. The VMD decomposes a real non-stationary signal $f\ (t)$ into different modes (sub-signal)/IMF such that it could offer specific sparsity properties during the reconstruction of the input signal $f\ (t)$ as presented in (3.1). A mode/IMF is defined as a time-varying amplitude and phase with sinusoidal behavior. It is also assumed that each mode, M is mostly compact around the central frequency [92].

$$f(t) = \sum_{m=1}^{M} f_m(t) = \sum_{m=1}^{M} B_m(t)\ cos(\phi_m(t)) \qquad 3.1$$

where $f\ (t)$ is an original signal, $f_m(t)$ is the mth mode of the decomposed signal, B_m is the amplitude of modulation, and ϕ_m is the phase modulation.

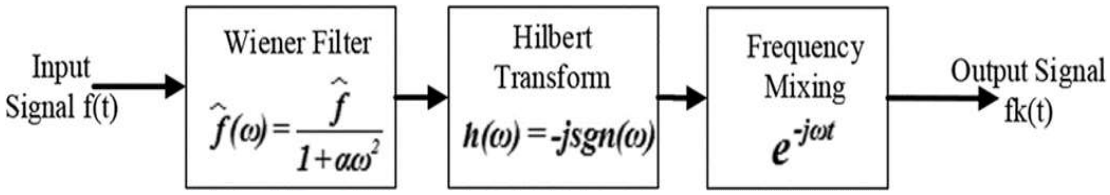

Figure 3.1 Basic block of VMD

The pictorial representation of the VMD is shown in Figure 3.1. It consists of four major components: Wiener filtering, the Hilbert transform, analytic signal, and frequency shifting through harmonic mixing. The step-by-step signal decomposition process is given in Table 3-1.

Table 3-1 Steps of signal decomposition

Step	Comments
Step 1	For each mode f_m, the Hilbert transform is used for converting the input (real) signal into an analytic signal. A single-sided frequency spectrum is obtained from an analytic signal.
Step 2	For each mode, the transformed signal at step 1 is mixed with an exponential tuned to the estimated central frequency of the respective mode to shift the frequency spectrum to the baseband.
Step 3	H^1 Gaussian smoothness has been used for computing the bandwidth of the signal. It has been computed using squared L^2-norm of the demodulated signal. formulated as shown in (3.2).

$$\min_{\{f_m\},\{\omega_m\}} \left\{ \sum_k \left\| \partial_t \left[\left(\delta(t) + \frac{j}{\pi t} \right) \times f_m(t) \right] e^{-j\omega_m t} \right\|_2^2 \right\} \ S.T. \ \sum_m f_m = f \qquad 3.2$$

where $\{fm\} = \{f\,1, \ldots, f_m\}$ and $\{\omega_m\} = \{\omega_1, \ldots, \omega_m\}$ are the modes and their central frequencies, respectively. This constrained quadratic problem is modified by using quadratic penalty α and Lagrangian multipliers to change a constrained problem to an unconstrained problem. Therefore, augmented Lagrangian $\mathcal{L}$ is introduced, and the modified relation can be expressed as (3.3) [94].

$$\mathcal{L}(\{f_m\},\{\omega_m\},\lambda) = \alpha \sum_m \left\| \partial_t \left[\left(\delta(t) + \frac{j}{\pi t}\right) \times f_m(t) \right] e^{-j\omega_m t} \right\|_2^2 + \left\| f(t) - \sum_m f_m(t) \right\|_2^2 + \left\langle \lambda(t), f(t) - \sum_m f_m(t) \right\rangle. \quad 3.3$$

To solve the above quadratic optimization problem and for the calculation of different modes and their central frequencies, an alternate direction method of multipliers [94]–[98] has been used. The solution of (3.3)is represented by (3.4) and (3.5).

$$\hat{f}_m^{n+1} = \frac{\hat{f}(\omega) - \sum_{i<m} \hat{f}_i^{n+1}(\omega) - \sum_{i>m} \hat{f}_i^{n}(\omega) + \frac{\hat{\lambda}^n(\omega)}{2}}{1 + 2\alpha(\omega - \omega_m^n)^2} \quad 3.4$$

$$\omega_m^{n+1} \leftarrow \frac{\int_0^\infty \omega |\hat{f}_m^{n+1}(\omega)|^2 d\omega}{\int_0^\infty |\hat{f}_m^{n+1}(\omega)|^2 d\omega} \quad 3.5$$

where f_m is the decomposed signal and ω_m is the central frequency. The solution obtained from (3.4) and (3.5) is in the spectral domain. Thereafter, an inverse Fourier transform has been employed for acquiring the time-domain signal for each mode f_m.

3.2.1 VMD: algorithm

The implementation of variational problem algorithm is given as follows:

Step 1:Intialize the$\{f_m\},\{\omega_m\}$ $\{\lambda\}$ for n=0

Step 2: Update the f_m, ω_m according to (3.3) & (3.4)

Step 3: Update the dual ascent λ according to (3.6)

$$\lambda^{n+1} = \lambda^n + \tau(\hat{f}(\omega) - \sum_m \hat{f}_m^{n+1}(\omega)) \quad 3.6$$

Step 4: Repeat until convergence ε is achieved according to (3.7).

$$\sum_k \left\|\hat{f}_m^{n+1} - \hat{f}_m^n\right\|_2^2 / \left\|\hat{f}_m^n\right\|_2^2 < \varepsilon \quad 3.7$$

The flow diagram for the implementation of the VMD problem is shown in Figure 3.2

3.2.2 Selection of VMD parameter

The VMD-based IDT has three parameters, namely, Lagrangian multiplier (λ), number of modes (M), and reconstruction fidelity factor (α).

(i) Lagrangian multiplier (λ): it is used for enforcing the constraint strictly. When the exact reconstruction of a signal is not required in the presence of noise, keep its value small or set to zero. This can be obtained by setting the update parameter to zero.

(ii) Number of modes (M): it is imperative to keep the number of modes appropriate to deal with over and under the binning of modes.

(iii) Reconstruction fidelity factor (α): it is kept at a smaller value for capturing a wide range of frequency components of the signal.

For ascertaining the islanding event, the three-phase voltage signals are decomposed into four modes (M = 4), which are decided by the fast Fourier transform of the voltage signal.

The voltage signal contains four frequency components that significantly impact the energy level. The reconstruction of a signal is not the motive of decomposition, so the reconstruction fidelity factor is kept moderate in the range of 2500.

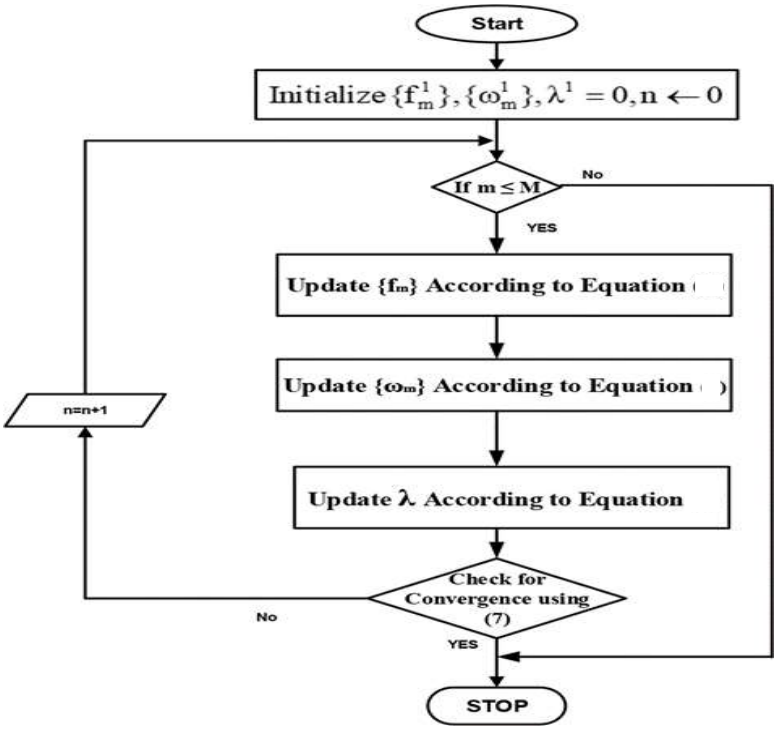

Figure 3.2 Flow diagram of VMD

3.3 IMPLEMENTATION OF THE PROPOSED VMD-BASED IDT

The acquired three-phase voltage signals at the interaction point of DG have been sampled and processed by VMD for computing the IMFs. The obtained IMFs have different components of frequencies. The IMF1 includes the fundamental frequency of the signal. The intermediate frequencies that appear during islanding are contained in IMF2. The IMF3 includes the higher frequency signals that can be useful in ascertaining switching transients, such as capacitor switching. Still, higher frequency signals that are normally noisy parts of signals are contained in IMF4. Therefore, IMF4 is never recommended for islanding detection under noisy conditions. The signal's noise part is

removed during its decomposition into the above-mentioned four modes. Thus, the only noise-free signals IMF1 through IMF3 can be utilized for the present application. The voltage signal, in this technique, is decomposed into IMFs of limited band ensembles. Since the VMD analysis is robust to noise and sampling frequency, its four modes decomposition could be used effectively under various conditions with different noise levels and sampling frequencies.

After the decomposition of the signals, the energy of the specific IMF is computed using (3.8). The event of islanding has been ascertained by comparing the computed energy level with the predefined energy threshold (ET) value

$$E(IMF_M) = \sum_{k=0}^{K-1} |IMF(k)|^2 \qquad 3.8$$

Here $E(\mathrm{IMF}_M)$ represents the Mth mode energy of IMF. K is the sample length of IMF, and k is the particular sample number. The flow chart of the proposed IDT has been shown in Figure 3.4.

The steps to be followed to implement the proposed VMD-based IDT are given in Table 3-2.

Table 3-2 Implementation of VMD based IDT algorithm

Step	Comments
Step 1	Acquire the three-phase voltage signals at the PCC of the target DG.
Step 2	Three-phase voltage signals have been processed through the VMD signal processing tool

Step 3	Four IMFs of the voltage signals have been obtained.
Step 4	Calculate the energy of IMF2 using (8).
Step 5	Is E(IMF2) ≥ ET. If yes, go to the next step, else go to step 1
Step 6	Islanding condition detected.
Step 7	Send trip command to DG.
Step 8	Stop.

3.4 SIMULATION RESULTS AND DISCUSSIONS

The performance of the proposed method has been tested on two test systems. The simulations of both the test systems have been carried out in PSCAD/EMTDC and MATLAB® 2017b, as shown in Figure 3.3. The proposed IDT has been executed on Intel(R) Core(TM) i3 4030 8 GB RAM 1.9 GHz processor. The 3−ϕ voltage signals have been sampled at the sampling frequency of 4 kHz. To demonstrate the proposed VMD-based IDT, some critical cases have been studied. The discrimination of islanding and non-islanding events has been done on the energy-based index proposed in this investigation. From the decomposed IMFs, IMF2 has been selected because it consists of zero signal components in the normal state. An energy-based performance parameter of IMF2 has been selected for the detection of islanding and non-islanding conditions.

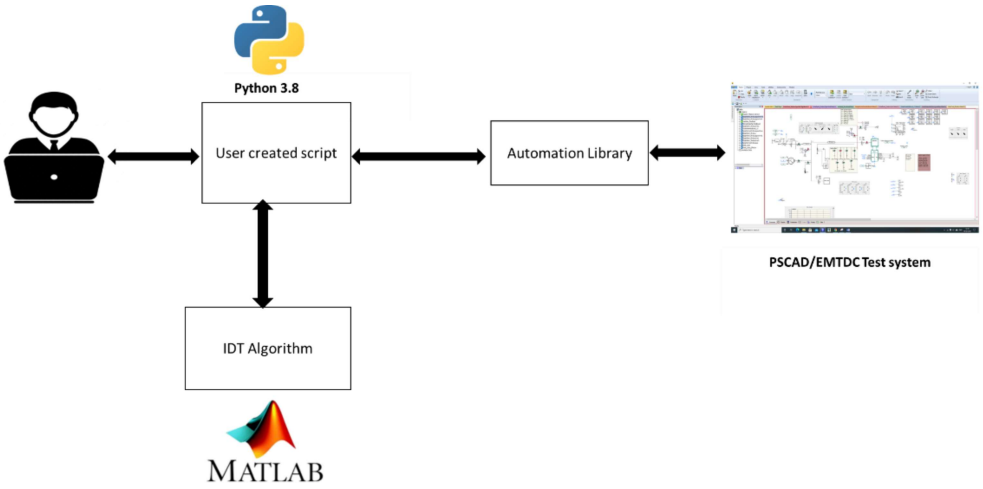

Figure 3.3 Off-line Simulation Platform

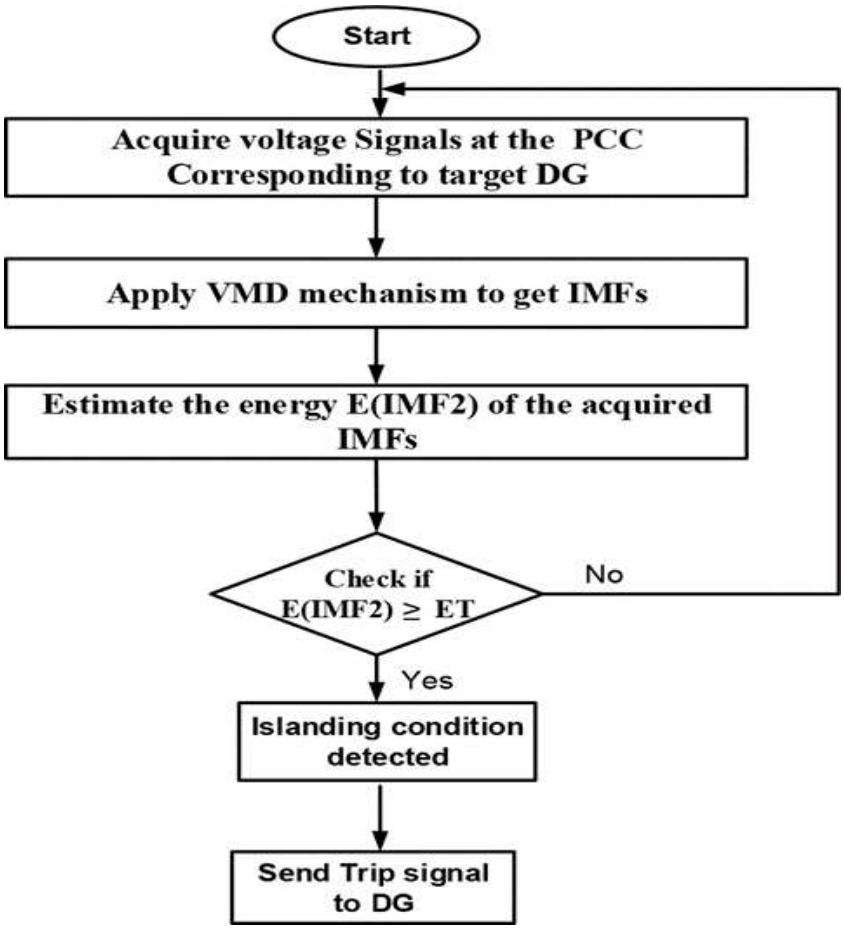

Figure 3.4 Flow chart of the proposed scheme for islanding detection

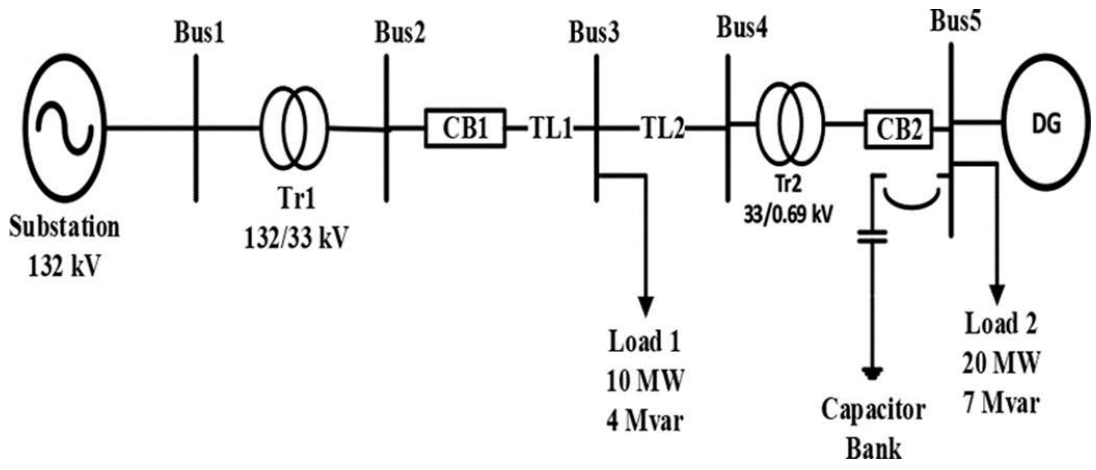

Figure 3.5 Modified five-bus test system

3.4.1 Test system I: five-bus system

To validate the proposed methodology, a five-bus test system has been considered. It consists of a 132 kV substation equipped with a step-down transformer having a rating of 100 MVA, 132/33 kV. Two loads are connected towards the secondary side at buses three and five. Besides, a DG set having a rating of 20 MVA is also connected at bus 5 with a 33/0.69 kV transformer. DG parameters, transformer, distribution line, and load have been adopted in [19] and are given in the Appendix. The single-line diagram of the system is depicted in Figure 3.5. The different operating scenarios have been created, and afterward, voltage and current waveforms have been captured at the point of interconnection of the DG. The power imbalance has been varied from 0 to 20% for active power and from 0 to 50% for reactive power. Different types of load impacts on islanding cases have been simulated. A total of 352 events have been simulated under the following two cases.

- Case 1: non-islanding (176 events): by load tripping, faults at different locations on the bus, capacitor switching, and induction machine switching.
- Case 2: islanding (176 events): by tripping CB1.

3.4.2 Non-islanding event

The simulation of the test system under normal operating conditions has been performed, and the voltage signals at the PCC (corresponding to the target DG end at bus 5) have been acquired. It is further processed through the VMD to obtain the IMFs. The decomposed signals, along with the original voltage signal, have been shown in Figure 3.6. It could be observed from the decomposed signals that there is no change in the IMF2 under normal conditions indicating the presence of almost zero signal component in IMF2. The energy of IMF2, E(IMF2) depicted in Figure 3.7 shows that under normal operation conditions, its energy value is zero.

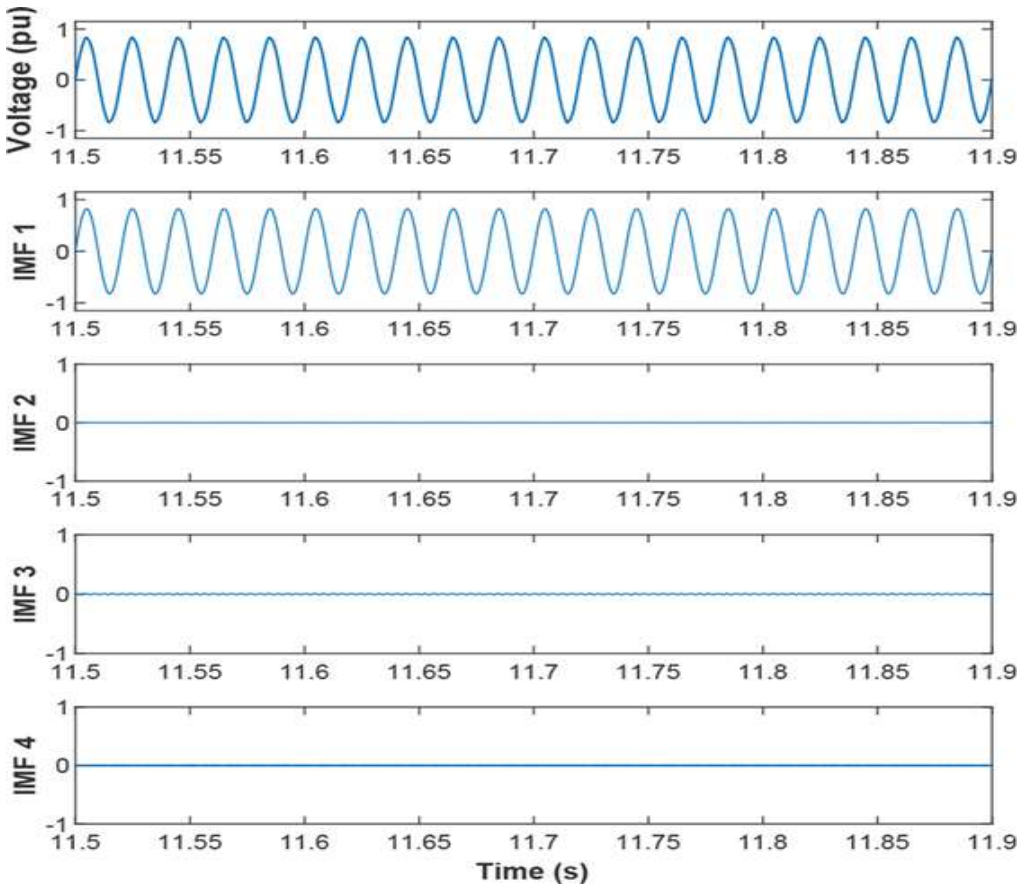

Figure 3.6 Decomposed voltage signals into IMFs

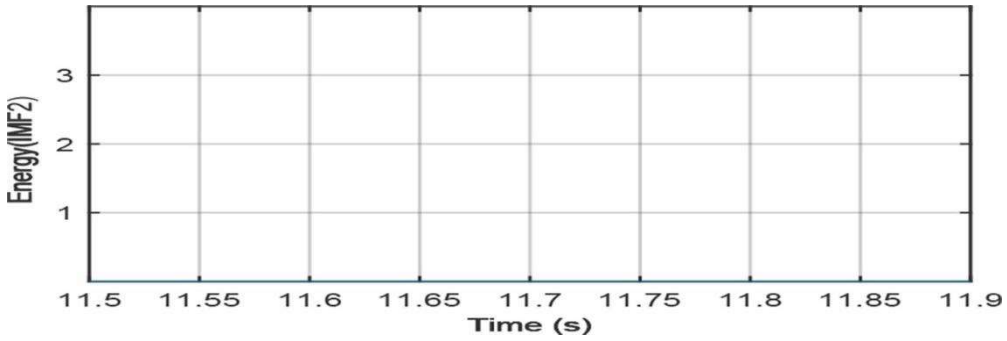

Figure 3.7 Energy plot of IMF2 under normal condition

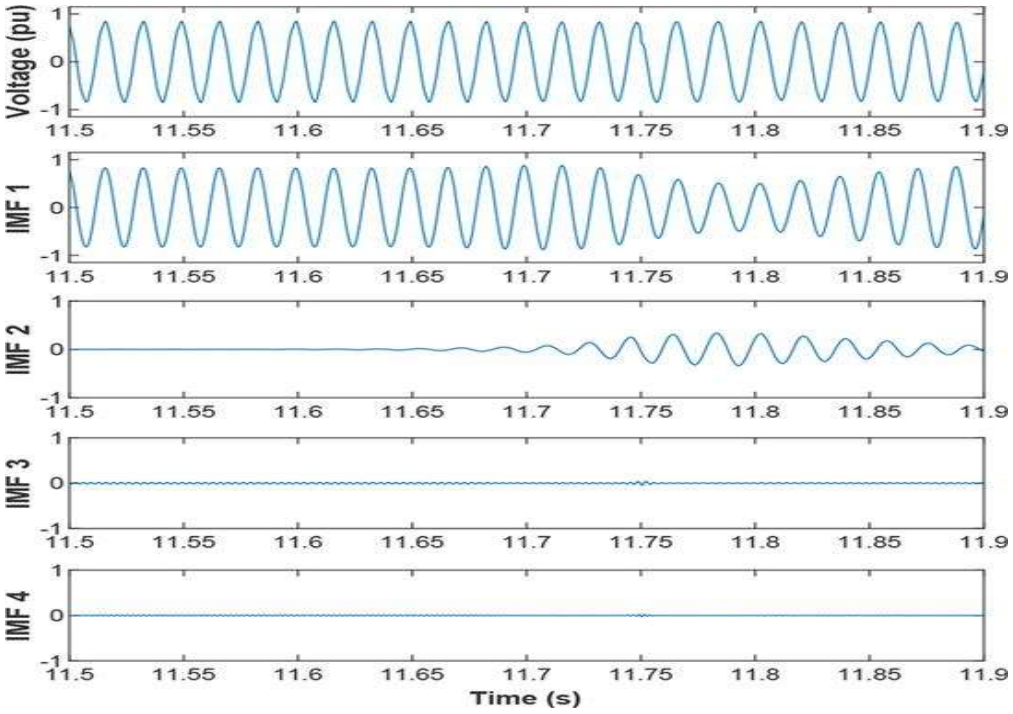

Figure 3.8 Decomposed voltage signal into IMF during islanding

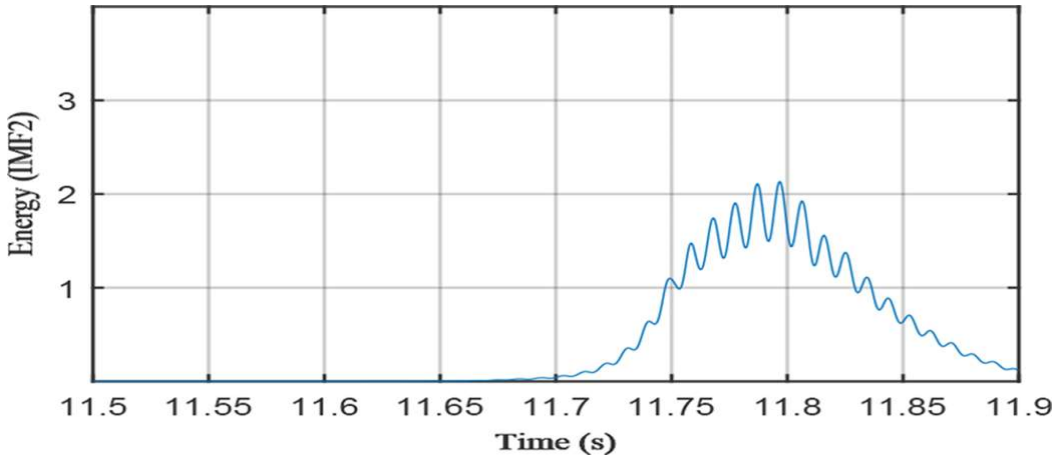

Figure 3.9 Energy of IMF2 during islanding

3.4.3 Islanding event

To analyze the islanding case, an islanding event has been simulated by opening circuit breaker CB1, shown in Figure 3.5. The breaker circuit is opened at the time instant of 11.68 s. As a consequence of the islanding event, the target DG end voltage would be impressed, and its IMFs would indicate the signature of the islanding incident at the instant when the grid is isolated from the rest of the system. The voltage signal and its IMF components obtained using the proposed VMD technique for the signal received from the target DG have been shown in Figure 3.8. Among the different IMFs, the IMF2 clearly shows the difference between healthy and islanded events. Comparing the IMF2 of two figures, Figure 3.6 and Figure 3.8, it could be observed that the IMF2 of Figure 3.8 has an islanding signature, and it could be used for the identification of the islanding event. As the IMF2-based energy parameter withholds the potential to identify the islanding event, therefore, the IMF2-based energy parameter has been utilized for islanding detection. The energy parameter obtained for IMF2 has been inked in Figure 3.9, from which it could be seen that there is an increase in the energy value from 11.68 s at which the islanding event takes place. Based on the energy value, an ET value can be defined such that whenever the energy value of the IMF2 parameter surpasses the ET, it would be classified as an islanding case, otherwise a non-islanding case.

3.4.4 ET selection

The energy-based performance parameter is calculated from IMF2 using (3.8) in the proposed IDT method. Due to the presence of components of high frequency, IMF2 carries a significant energy content during DG unit islanding. Whereas the IMF2 energy content changes by a small amount in the case of other non- islanding events such as a switching phenomenon. Moreover, an almost negligible magnitude of IMF2 is observed

under the healthy condition, as discussed in the previous section. It is further noticed that the magnitude of the voltage signal's IMF2 component suddenly increases at every event, irrespective of islanding or other abnormal events. Subsequently, the IMF2 signal's energy content will change. This change in the energy content would be different for different events. Therefore, a discriminating threshold value is desired to distinguish between non-islanding and islanding events. In the present study, this value has been recognized by the ET, a discriminating range, i.e., the threshold has been identified to discriminate between the non-islanding and islanding states. However, this threshold would be system-dependent. Therefore, an appropriate selection of the threshold is paramount for the method's proper and reliable discriminating property. To arrive at a proper distinction, a large number of studies have been carried out. The ET has been chosen based on the energy magnitude under critical islanding and non-islanding events, i.e., under the condition of zero power mismatch, switching of load, and fault event considering different target DGs. The maximum energy of IMF2 under various conditions of both the test systems has been calculated, and their maximum energy has been tabulated in Table 3-3 and Table 3-4. The energy value is the highest in the non-islanding case in the LLLG fault case, which is 1.615 for the test system I, as tabulated in Table 3-3. The highest energy value for the non- islanding event for test system II is 1.2202, as given in Table 3-4. The minimum energy for the islanding event is under zero power mismatch conditions for the test systems I and II are 2.133 and 2.03, respectively. So the selection of the ET value has to be > 1.615 and < 2.03. The threshold value of 2 has been chosen to be the most suited value, observing the simulated results of various types of cases. It is mentioned that in both the test systems, the voltage signal has been used for VMD decomposition in per unit (p.u.).

Table 3-3 Maximum energy for various cases of test system I

Sl.	Event	Maximum Energy(IMF2)
	Non-Islanding case	
1.	Normal case	1.45×10^{-5}
2.	Capacitor switching	8.72×10^{-4}
3.	Dynamic load(Induction Machine) switching	0.002923
4.	LG fault(away from PCC)	0.576
5.	LLG fault(away from PCC)	0.5663
6.	LG fault at PCC bus2	1.287
7.	LG fault at bus 5	0.08717
8.	LLG fault at bus 5	1.445
9.	LLG fault at bus 2	0.1243
10.	LLLG bus2	0.616
11.	LLLG bus5	1.615
12.	LL bus2	1.519
13.	LLbus5	0.4547
	Islanding case	
14	Zero power mismatch	2.133
15	Case1(High mismatch)	7.478
16	Islanding capacitor switching	5.651
17	Islanding with load rejection(66%)	11.25
18	Islanding with load rejection(33%)	19.02
19	Islanding with voltage-dependent load	8.171
20	Islanding with frequency-dependent load	7.728
21	Islanding +5% RPM	6.617
22	Islanding +5% APM	7.303
23	Islanding -5% RPM	3.348
24	Islanding -5% APM	3.042
25	Islanding +10% RPM	3.478
26	Islanding +10% APM	2.268
27	Islanding -15% RPM	5.237
28	Islanding -15% APM	4.667

Table 3-4 Maximum energy for various cases of test system II

Sl.	Event	Maximum Energy(IMF_2)
	Non-Islanding case	
1.	Normal case	2.8×10^{-5}
2.	Capacitor switching (5.5 MVAr)	0.0066
3.	Dynamic load(Induction Machine) switching	0.0265
4.	LG fault	1.1348
5.	LLG fault	1.1017
6.	LL fault	0.5018
7.	LLLG fault	1.2202
	Islanding case	
8.	Zero power mismatch	2.037

9.	Islanding capacitor switching	5.651
10.	Islanding presence of synchronous DG	10.588
11.	Islanding with frequency-dependent load	4.9788
12.	Islanding +5% RPM	4.617
13.	Islanding +5% APM	5.303
14.	Islanding -5% RPM	3.348
15.	Islanding -5% APM	3.2769
16.	Islanding +10% RPM	4.859
17	Islanding +10% APM	5.0365

3.4.5 Capacitor switching event

Capacitor banks are switched on and off regularly to improve the power factor of the distribution network. Such events cause fluctuation in voltage signals. Distinguishing the switching event from the islanding event is critical in such cases. To demonstrate such ability of the proposed method, the 11 MVAR capacitor banks connected at bus 3 have been switched ON at 11.75 s, as shown in Figure 3.10. In Figure 3.10, it is shown that the small perturbation takes place at a capacitor-switching instant, as seen in IMF2. The energy of IMF2 shown in Figure 3.11 illustrates that the energy has been much less than that of ET at the time of capacitor switching.

3.4.6 Simultaneous capacitor switching and islanding events

This is another scenario created where capacitor switching and islanding occur simultaneously at 11.68 s. In this case, the energy value crosses the threshold after islanding at 11.77 s. The energy function plot has been depicted in Figure 3.12 for this case. The decision time required for islanding detection by the proposed algorithm is 0.09 s. This indicates the speed of detection by the proposed IDT method.

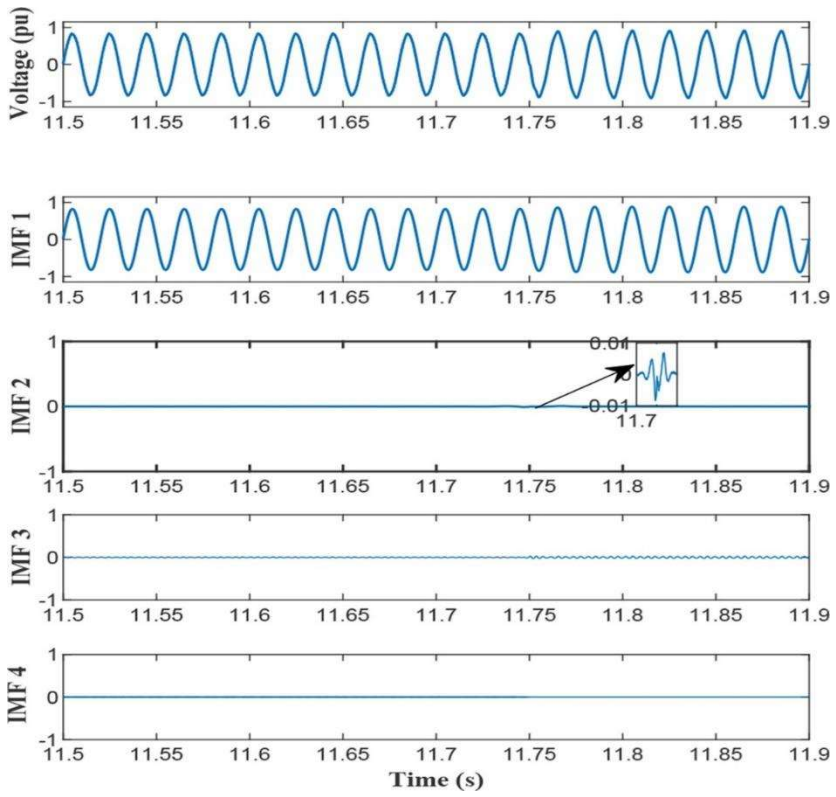

Figure 3.10 Decomposed voltage signal during a capacitor switching event

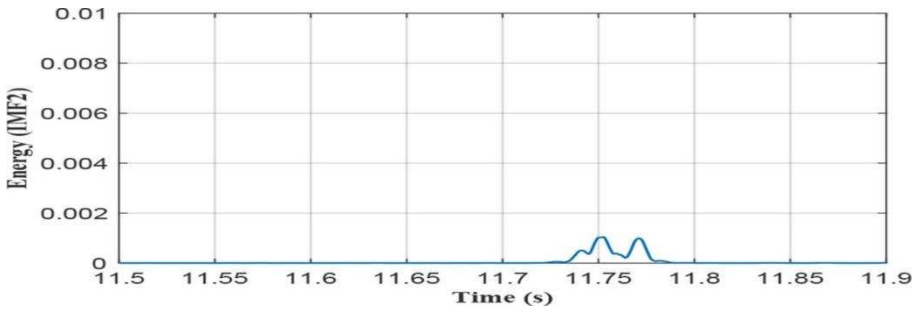

Figure 3.11 Energy of IMF2 during capacitor switching

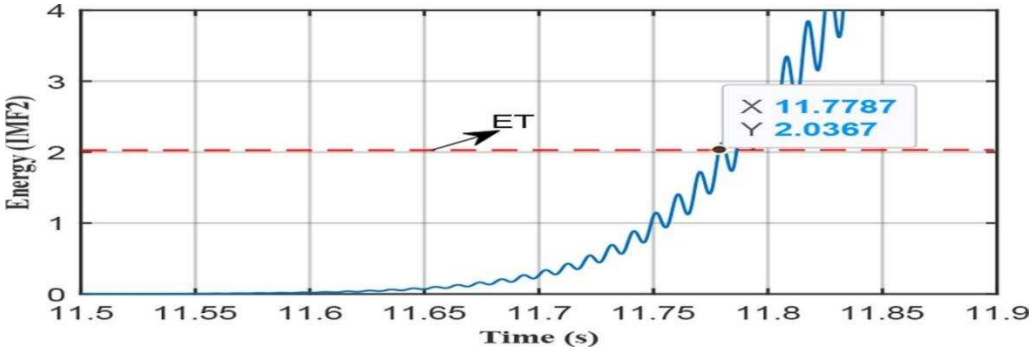

Figure 3.12 Energy of IMF2 during subsequent capacitor switching and islanding

3.4.7 Load-switching events

In an active distribution network, the net load changes dynamically. To evaluate the performance of the proposed IDT method, an investigation of sudden load switching at PCC has been carried out. A case has been simulated where 33% of the total load is disconnected at 11.5 s and connected at 11.55 s. Again 66% of the total load has been tripped at 11.6 s and reconnected at 11.65 s. The energy variation in this scenario has been shown in Figure 3.13. In this case, the energy is lower than the set value of ET (i.e., 2) for islanding. A significantly less value of the energy of IMF2 under load switching shows that the load variation has a negligible impact on the proposed scheme. Hence, it could be comprehended that the proposed IDT is immune to variation of loads.

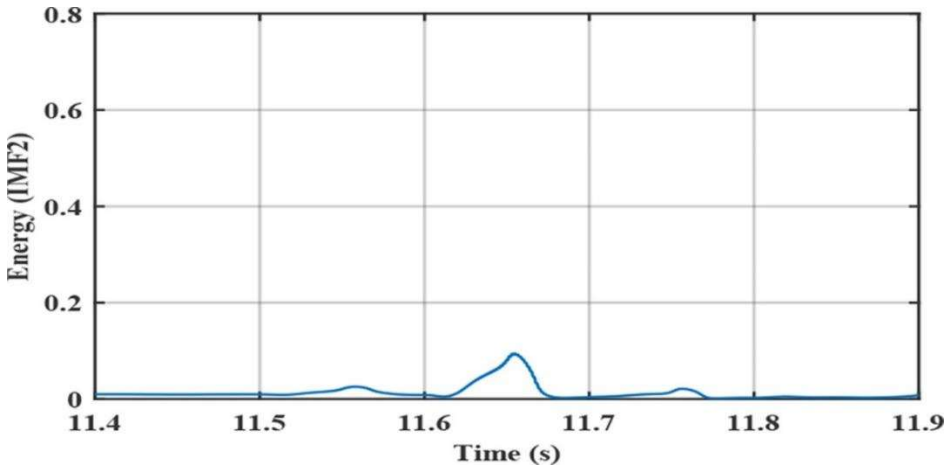

Figure 3.13 Energy of IMF2 during a load switching event

3.4.8 Simultaneous load rejection and islanding events

Under this case, two scenarios have been simulated. Under the first scenario, 33% load is rejected at the time of islanding at 11.68 s. The energy variation in this scenario has been shown in Figure 3.14(a). In this case, also the energy value crosses the ET value of 2 sets for islanding. Another such scenario has been created by the simultaneous rejection of 66% of total load and islanding at 11.68 s. In this case, also the energy values crossed the

ET value of 2, as shown in Figure 3.14(b). It could also be observed from Figure 3.14 (a) and (b) that the energy value crossed the threshold at 11.70 and 11.69 s in both scenarios, respectively. It has been maintaining the speed of islanding detection of 0.02 and 0.01 s. Thus, it has successfully detected the islanding in 0.02 and 0.01 s, respectively, in the first and second cases.

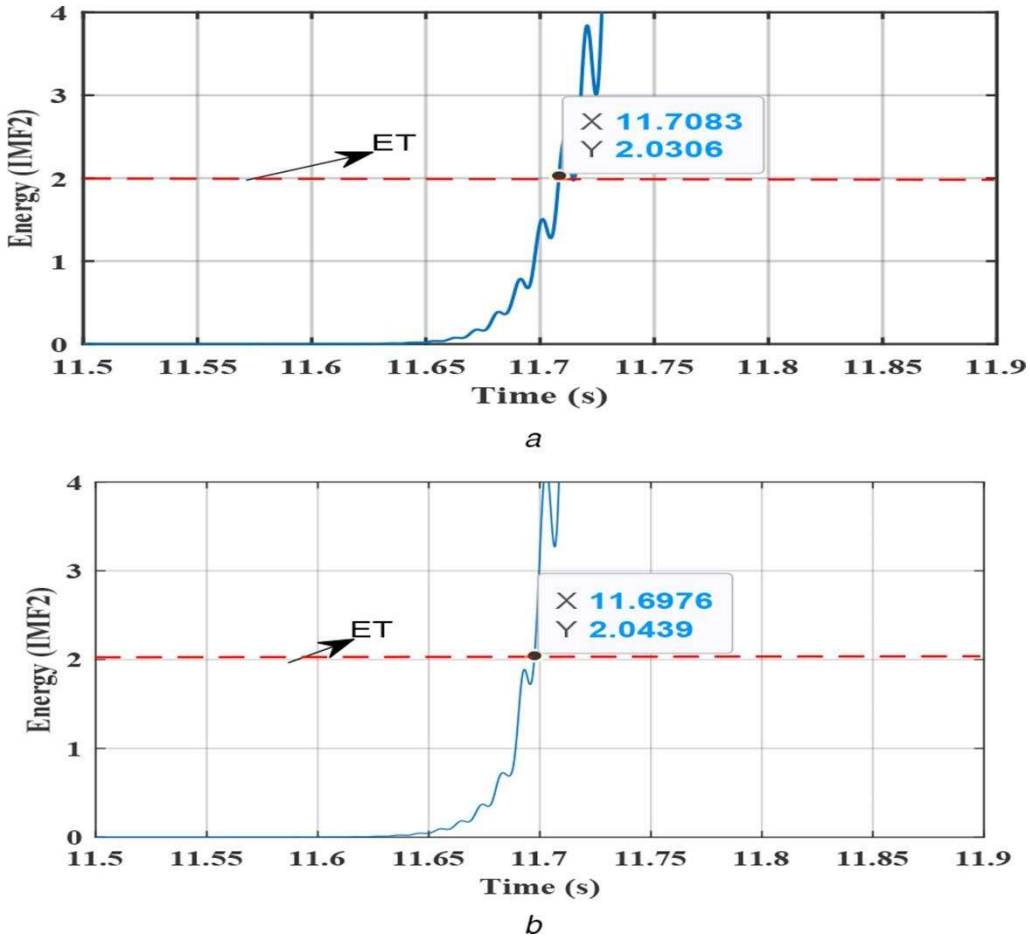

Figure 3.14 Energy plot of IMF2 (a) 33% of total load rejection, (b) 66% of total load rejection

3.4.9 Fault events

It is expected that an islanding protection relay set should be well competent in discriminating between islanding and fault events. The islanding relay should effectively identify the fault case as a non-islanding event and prevent DG tripping in the distribution network. The efficacy of the proposed IDT has been thoroughly investigated under

multiple fault conditions simulated on the five-bus system shown in Figure 3.5. The fault events have been created at 11.75 s for a time span of 0.05 s. The acquired DG side voltage samples during line-to-ground (LG) and double-line-to-ground (LLG) fault events have been shown in Figure 3.15 (a) and (c), and similarly for line-to-line (LL) and LLLG events are depicted in Figure 3.16 (a) and (c). These acquired samples have been processed through the proposed VMD mechanism, and the energy of IMF2 has been computed. The estimated variation of energy for all the above-discussed fault events has been depicted in Figure 3.15 (b), (d) and Figure 3.16 (b), (d) for LG, LLG, LL, and LLLG faults, respectively. It can be easily observed that the estimated energy level during all considered fault cases is below the set ET value for non- islanding events. Hence, it has been reaffirmed that the proposed IDT effectively discriminates between the fault and the islanding event.

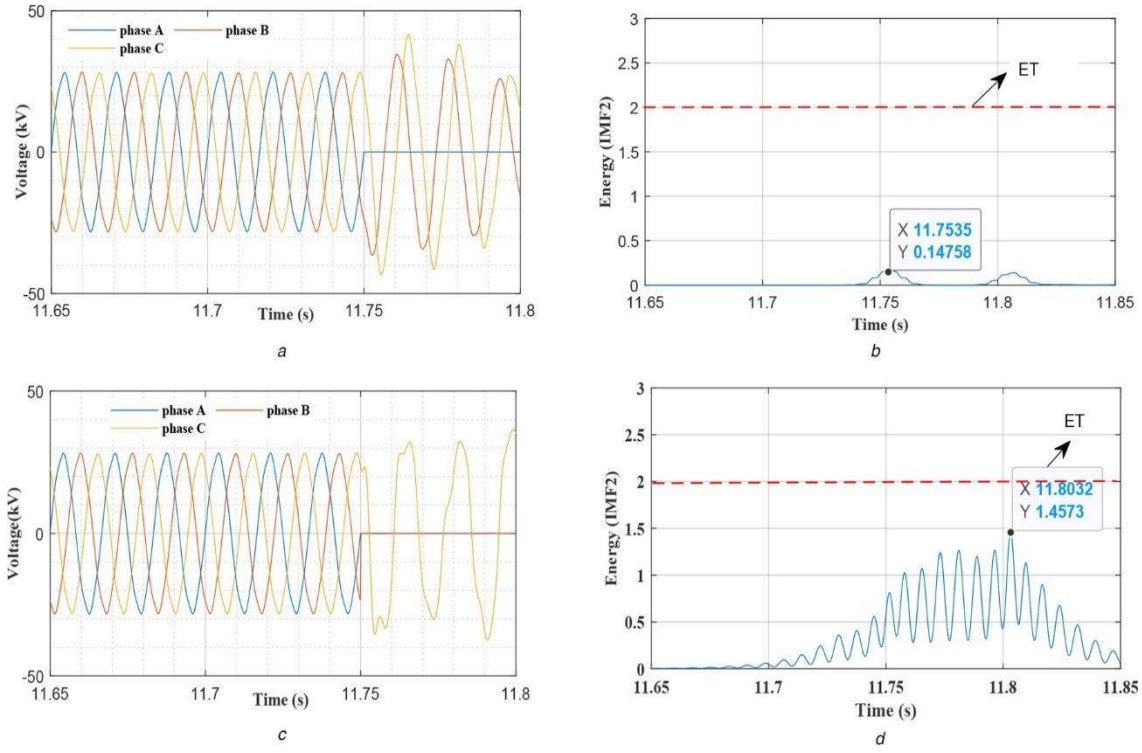

Figure 3.15 Performance of the proposed IDT during fault inception of bus 5 (a) Target DG end voltage during LG fault, (b) Energy of IMF2 during LG fault, (c) Target DG end voltage during LLG fault, (d) Energy of IMF2 during LLG fault

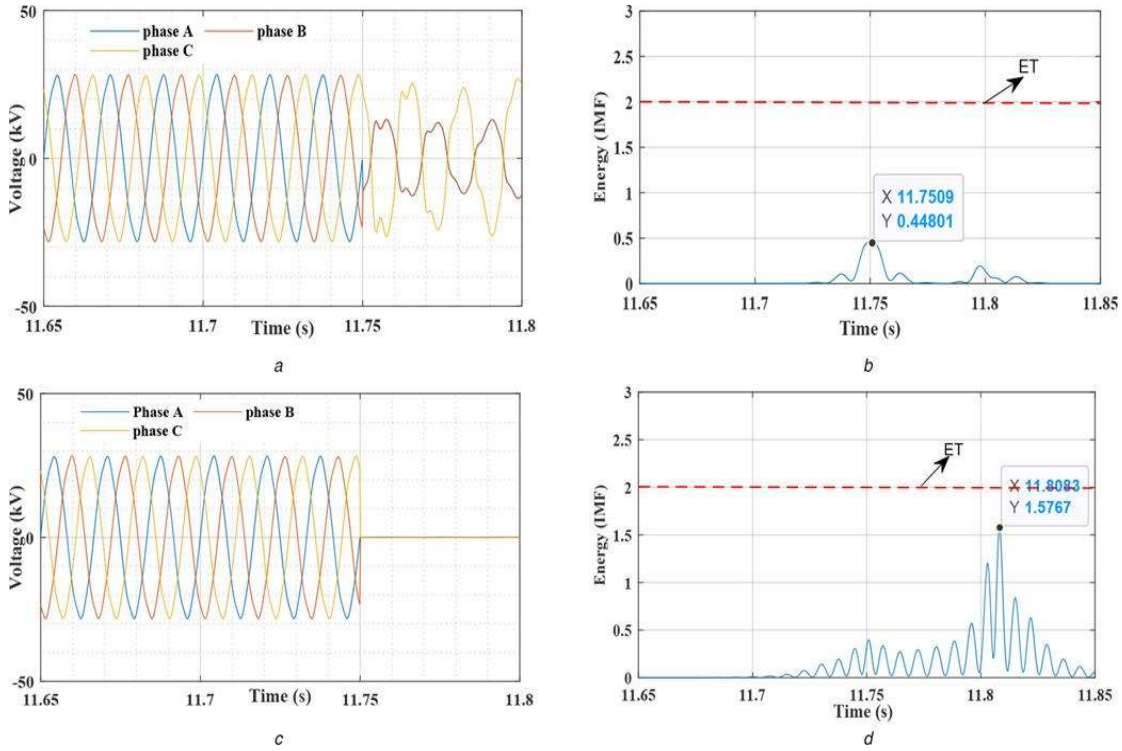

Figure 3.16 Performance of the proposed IDT during fault inception of bus 5 (a) Target DG end voltage during LL fault, (b) Energy of IMF2 during LL fault, (c) Target DG end voltage during LLLG fault, (d) Energy of IMF2 during LLLG fault

3.4.10 Assessment of performance of the proposed method on other kinds of load and operating conditions

From the analysis of the previous sections, the efficacy of the proposed method is proven. The method is accurate and fast for various test cases of islanding and non-islanding events. However, it is further required to check the performance of the proposed method in events of crucial and complex operating conditions of the DG. In this section, different dynamic loads and active and reactive power mismatch (APM and RPM) cases in the power network have been simulated for demonstration.

3.4.10.1 *Dynamic load switching events*

In this case, an induction machine of 5 MVA rating has been switched in 11.75 s at PCC. The acquired voltage signal has been shown in Figure 3.17 (a). This signal has been

processed through the proposed IDT, as shown in Figure 3.17 (b), whereby energy variation has been inked. Figure 3.17(a) shows a voltage dip at the time of switching, but very less energy variation of IMF2 has been observed, as shown in Figure 3.17(b). Thus, the proposed IDT successfully differentiates between starting transient and islanding phenomena.

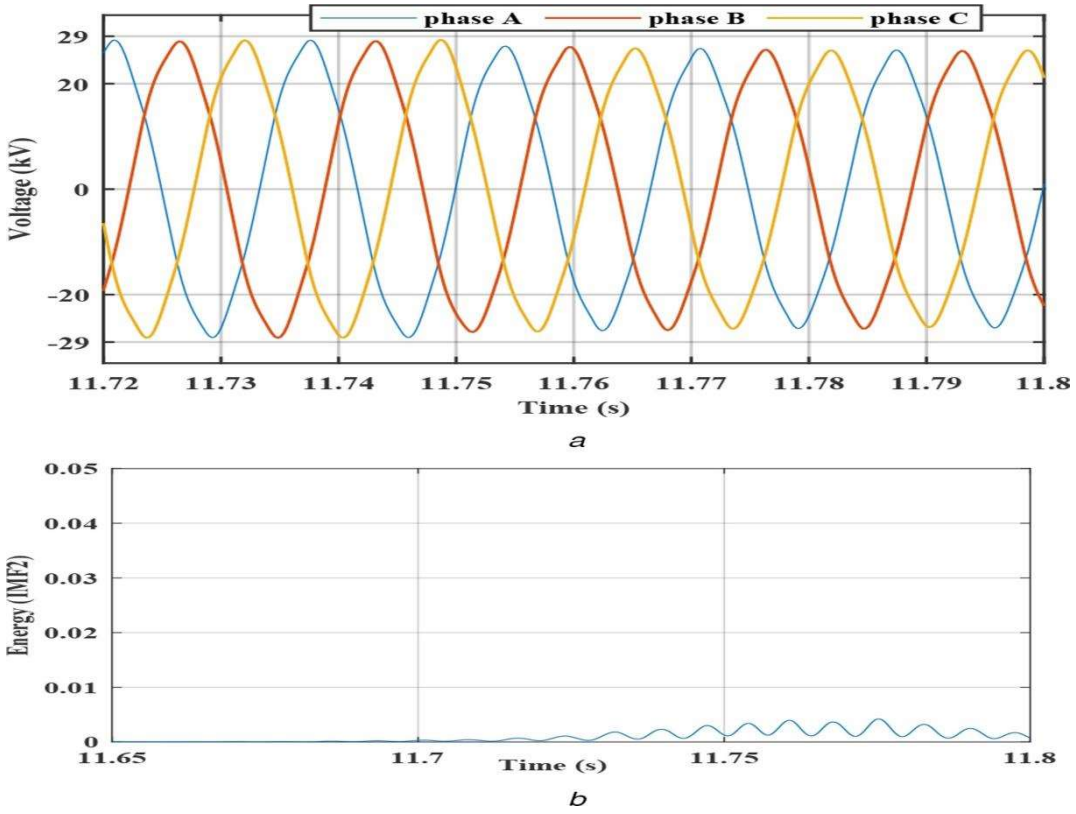

Figure 3.17 Performance of the proposed IDT during switching of an induction machine (a) Voltage signal of DG end, (b) Energy of IMF2 of the decomposed signal

3.4.10.2 *Active and reactive power mismatch*

To further evaluate the proposed method's performance, various zero power mismatch, APM, and RPM conditions have been simulated between the grid and DG by the varying PCC load. The following cases have been simulated.

- APM: at the PCC, the load is varied to create an APM of 0–10% under islanding conditions maintaining an RPM of 5%.

- RPM: The reactive power mismatch is varied from 0 to 20% while maintaining an APM of 5% for all islanding events.

Under NDZ conditions, when the RPM and APM between the grid and DG are 0%. Under such a condition, zero power flows between the main grid and DG system, which poses a challenge for the detection of islanding for the conventional relays, but the proposed IDT has successfully ascertained islanding under a zero mismatch condition as shown in Figure 3.18 (a). The proposed islanding ascertaining mechanism is capable of detecting islanding under various real and RPM conditions depicted in Figure 3.18 (b) and (c).

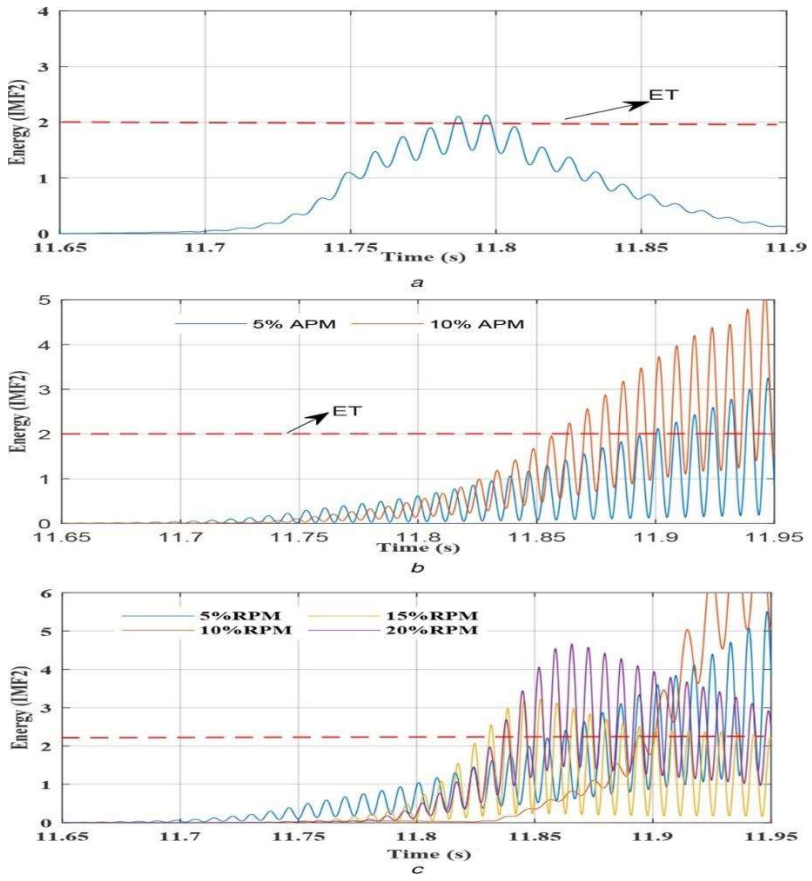

Figure 3.18 Performance of the proposed IDT under various critical mismatch conditions (a) Zero power, (b) APM, (c) RPM

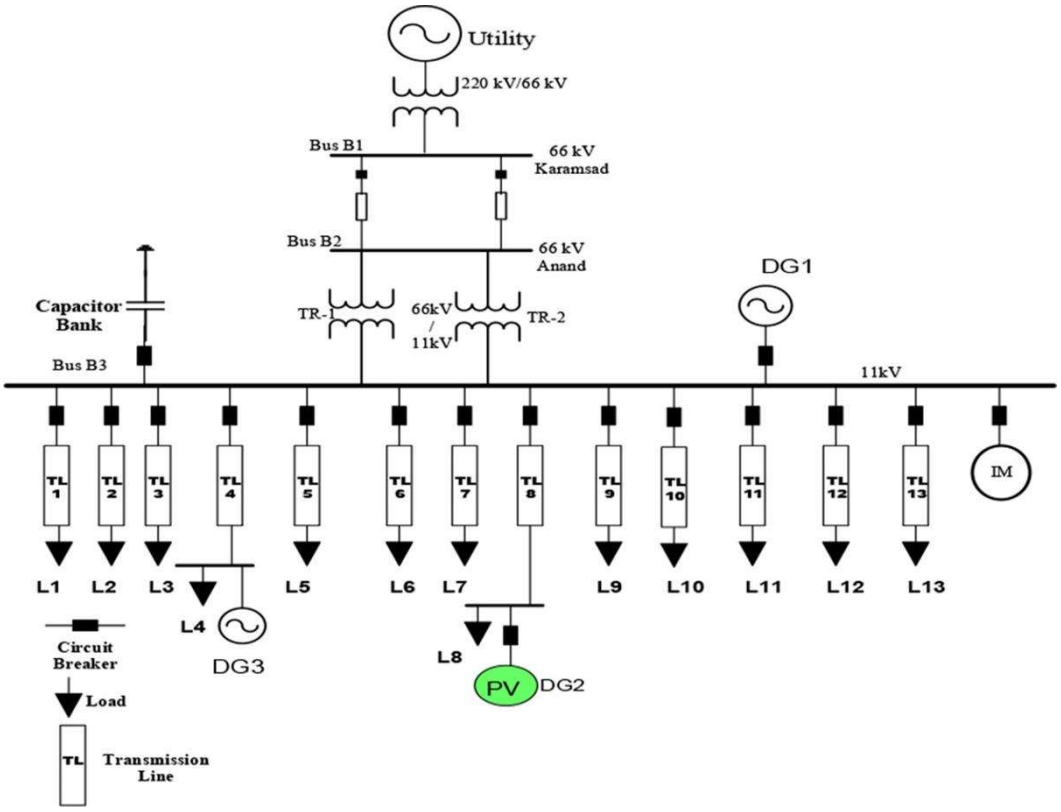

Figure 3.19 Single line diagram of a practical distribution network

3.4.11 Test system II: practical distribution system

For vindicating the efficacy of the proposed IDT, it has also been applied to a real distribution network. The single-line representation of the same has been demonstrated in Figure 3.19. The network has been modified by adding three DGs into the system. DG1 and DG3 are interconnected to an 11 kV bus and feeder 4 at the end of the TL4. DG2 is connected to feeder 8 at the end of the TL8. DG1 and DG3 are synchronous generator types, and DG2 is an inverter-based DG. In the present study, DG2 has been taken as a photovoltaic (PV)-type DG. The data of transformers, transmission line parameters, and load details are adopted from [13]. The utilized DG parameters are provided in the Appendix. Multiple cases of fault scenarios, islanding, and other critical contingencies have been simulated and tested on the designed real distribution system. The details of

all considered cases are provided in Table 3-5. A total of 356 cases have been simulated under various islanding and non-islanding events.

Table 3-5 Types of events

Sl.No	Cases	Events
1	Islanding	transformer 220/66 kV CB tripping, 66 kV both transmission line CB tripping, transformer 66 / 11kV CBs tripping, TL8 CB tripping
2.	Non-islanding	capacitor switching, load switching, induction motor switching, faults (LG, LL, LLL), DG tripping excluded target DG

Figure 3.20 shows that the proposed islanding ascertaining mechanism effectively detects the zero power mismatch condition. The performance of the proposed IDT under different fault events is shown in Figure 3.21. The fault incepts at 5.5 s for a duration of 0.05 s, and then it is cleared. The ET values under different considered fault cases shown in Figure 3.21 are lower than the threshold value (i.e., 2). This reaffirms that the proposed method has been competent in ascertaining the islanding events even in any intricate practical distribution system.

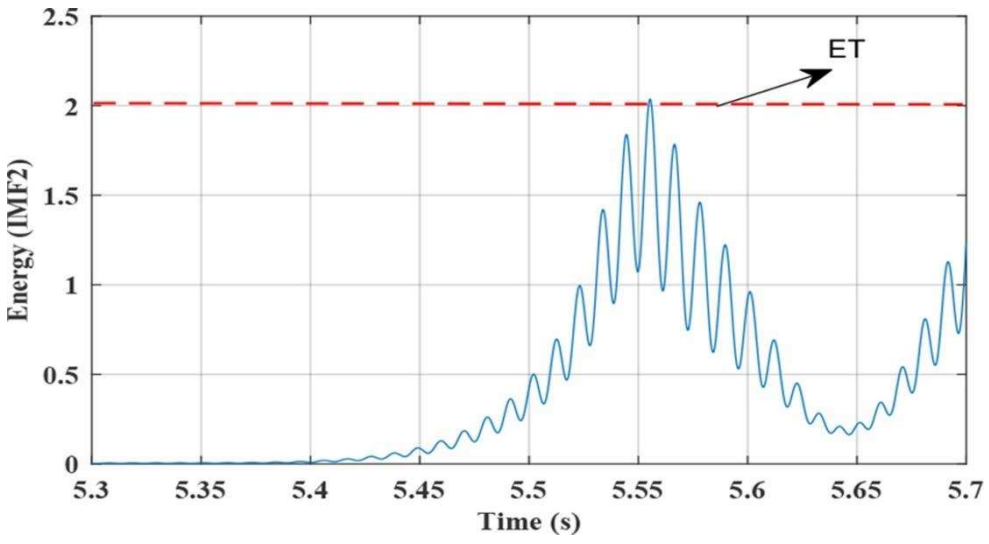

Figure 3.20 Energy of IMF2 during islanding under zero power mismatch condition for practical distribution system

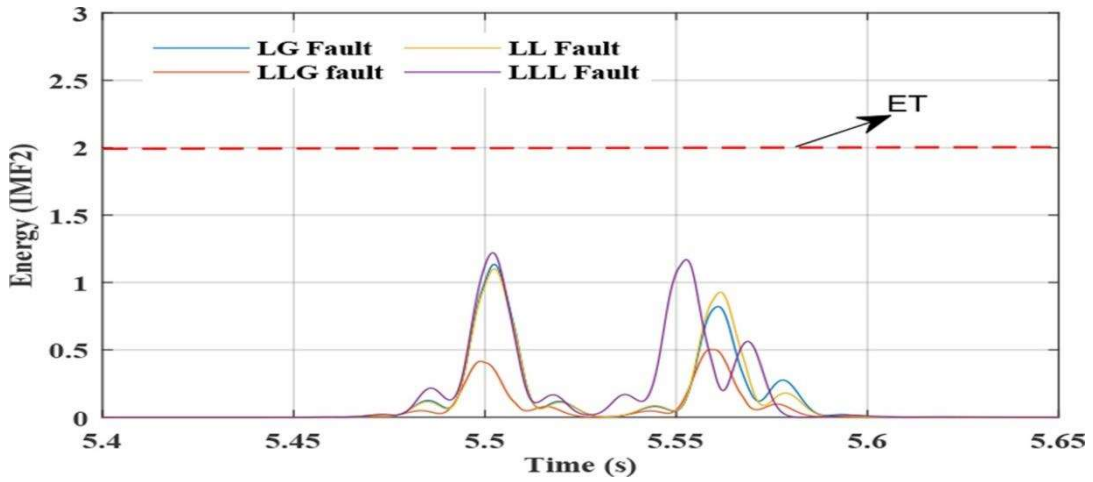

Figure 3.21 Energy of IMF2 for LG, LLG, LL, and three-phase (LLL) faults in a practical distribution system

3.5 SUMMARY

A novel adaptive islanding detection mechanism based on the variational mode decomposition of voltage samples has been proposed and implemented in the present investigation. The VMD technique has been applied for estimating the IMFs of the acquired voltage signals at the interaction point of the target DG. The performance of the proposed VMD-based islanding ascertaining mechanism has been corroborated by testing it on a five-bus network under different transforming conditions such as islanding, non-islanding, and some critical cases. The test results demonstrated that the proposed islanding ascertaining mechanism is capable of identifying various events, including critical cases. The prime attribute of the proposed mechanism includes its immunity to an external noise signal and a robust signal processing-based IDT that comprehensively mitigated NDZ. The efficacy of the proposed method has also been tested on a real distribution network having multiple DGs. The testing outcomes reaffirm that the proposed IDT is competent in ascertaining the islanding events, and it is also well effective for multiple DG networks.